

7

Proportional counters

7.1 Basic principles

A relativistic charged particle releases around 100 electron–ion pairs per cm in a gas at NTP. In a simple two-electrode parallel plate structure with a capacitance of a few tens of pF, the collection of this charge would produce a voltage signal of a few μV , below the possibility of detection with simple electronics means. As discussed in the previous chapter, application of a high electric field between the electrodes results in avalanche multiplication, boosting the signal amplitude by many orders of magnitude. Thanks to their simple construction, parallel plate or avalanche counters have been used in the past, and with several improvements are still widely used in particle physics to cover large detection areas (see Chapter 12); they suffer, however, from one basic limitation: the detected signal depends on the avalanche length, i.e. from the point of release of the primary ionization, implying a lack of proportionality between the energy deposit and the detected signal. Also, due to the large statistical fluctuations in the avalanche size, the Raether condition is occasionally met even at moderate gains, leading to breakdown.

Developed in the early years of the last century (Rutherford and Geiger, 1908), a cylindrical coaxial geometry for the counter overcomes these limitations and provides an amplified signal proportional to the initial ionization (Figure 7.1). A thin metal wire is stretched on the axis of a conducting cylinder and insulated from it, so that a difference of potential can be applied between the electrodes, with the central wire (the anode) positive in respect to the outer cylinder (the cathode).

The electric field in the tube is highest at the surface of the wire, and rapidly decreases towards the cathode (Figure 7.2); using thin wires, very high values of field can be obtained close to the anode. In most of the volume where the charges are produced by the primary interaction processes, the electric field only makes electrons and ions to drift respectively towards the anode and cathode.

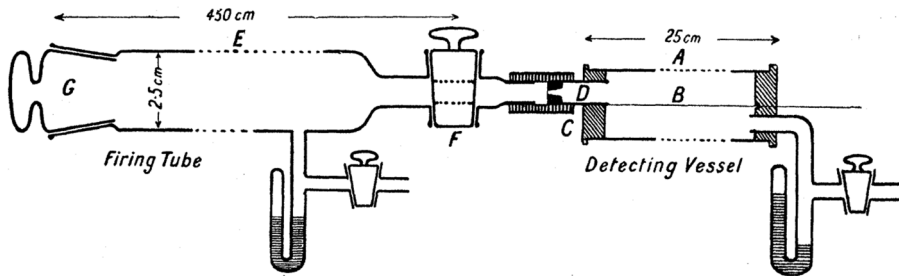


Figure 7.1 The original design of the proportional counter. Ionization electrons released by a radium sample are let into the detecting vessel, multiplied and detected (Rutherford and Geiger, 1908).

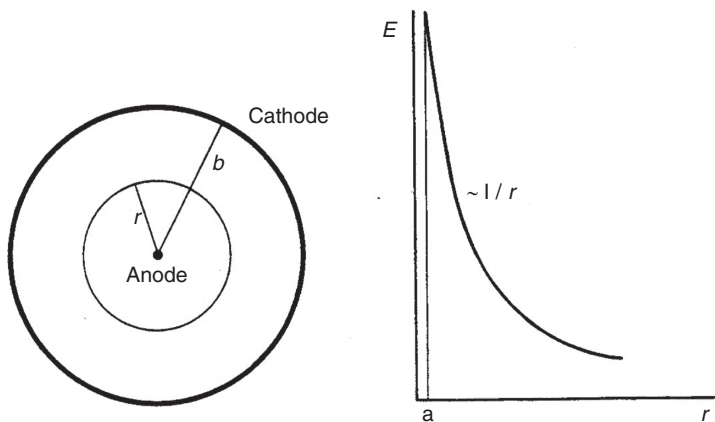


Figure 7.2 Schematics of a proportional counter and its field.

On approaching the anode, normally at a distance of a few wire radii, electrons begin experiencing a field strong enough to initiate charge multiplication; an avalanche develops, with electrons in the front and ions behind, as in the parallel plate case, but with a fast decreasing value of the mean free path for multiplication. Because of lateral diffusion and the small radius of the anode, even at moderate gains the avalanche tends to surround the wire, as shown schematically in Figure 7.3; due to the large difference in drift velocity, electrons in the front are quickly collected, while positive ions slowly drift towards the cathode. As will be seen later, most of the detected signal is due not to the collection of electrons, but to the initially fast motion of the ions receding from the anode, where most of them are produced.

The design and operation of wire proportional counters have been extensively described in articles and textbooks (Rossi and Staub, 1949; Curran and Craggs, 1949; Wilkinson, 1950; Korff, 1955).

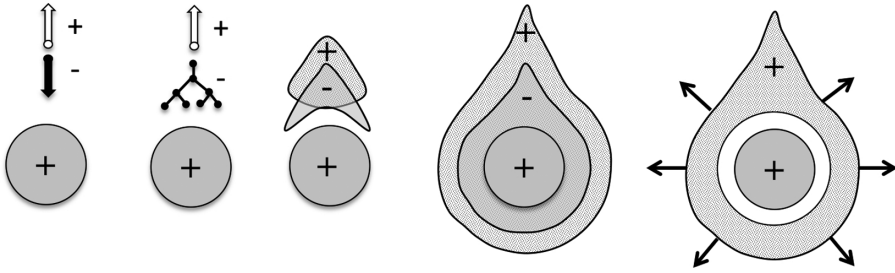


Figure 7.3 Avalanche growth around a thin wire.

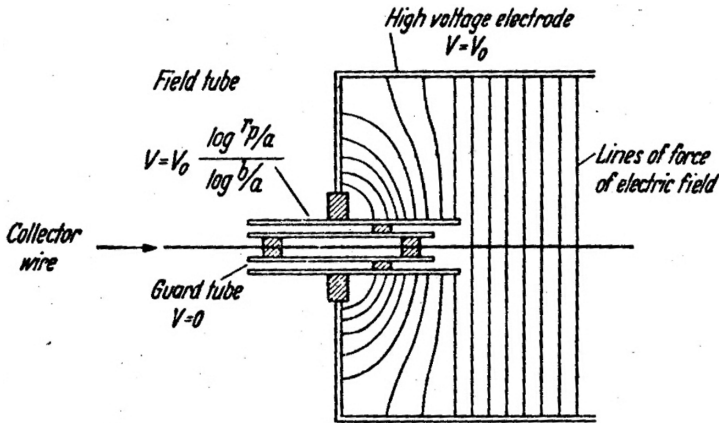


Figure 7.4 Wire holder and guard ring structure on a proportional counter edge (Cockroft and Curran, 1951). By kind permission of the American Institute of Physics.

To prevent edge discharges and delimit the active volume of the counter to the region of uniform response, one or more additional electrodes or guard rings are usually added at the edges of the counters; Figure 7.4 shows a classic configuration (Cockroft and Curran, 1951). A thin anode wire is mounted within a metallic tube, insulated from it and kept at the same potential. A second coaxial tube of larger diameter, insulated from the previous, receives a voltage corresponding to the potential present in that position within the active volume of the counter. The guard rings collect charges released in the region close to the wire's end, and ensure a uniform response of the sensitive volume.

Figure 7.5 (Montgomery and Montgomery, 1941) shows a typical dependence of detected charge on anode voltage in a proportional counter, for two sources of radiation differing in primary ionization density. At very low voltages, charges start being collected, but recombination is still a dominant process; at higher fields, full charge collection begins, and the counter is said to operate in the ionization chamber

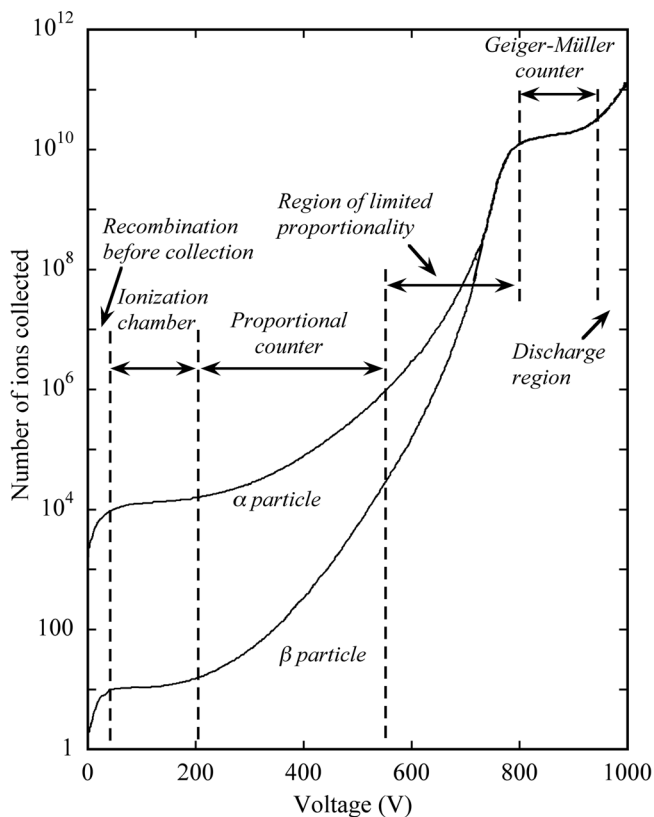


Figure 7.5 Voltage dependence of detected charge in a proportional counter (Montgomery and Montgomery, 1941). By kind permission of Elsevier.

mode. Increasing the voltage further, and above a threshold value V_T , the electric field close to the surface of the anode gets large enough to initiate a process of charge multiplication; gains in excess of 10^5 – 10^6 can be obtained, with the detected charge proportional, through the multiplication factor, to the original deposited charge. At even higher voltages, however, this proportionality is gradually lost, as a consequence of the electric field distortions due to the large charge density building up around the anode; the region of limited proportionality ends in a region of saturated gain, where the detected signal is independent of the original ionization density.

When the voltage is further increased, various secondary processes set in, resulting in breakdown or, under special conditions (low pressure, poorly quenched gases) in a photon-mediated propagation of the multiplication over the full length of the anode, the so-called Geiger–Müller operation.

If a and b are the radii of anode and cathode the electric field and potential at a distance r from the centre of the counter are:

$$E(r) = \frac{CV_0}{2\pi \epsilon_0 r} \quad \text{and} \quad V(r) = \frac{CV_0}{2\pi \epsilon_0} \ln \frac{r}{a}. \quad (7.1)$$

$V_0 = V(b)$ is the overall potential difference, with $V(a) = 0$; ϵ_0 is the dielectric constant (for gases $\epsilon_0 = 8.86$ pF/m), and C the capacitance per unit length of the counter:

$$C = \frac{2\pi \epsilon_0}{\ln(b/a)}. \quad (7.2)$$

Following Rose and Korff, the multiplication factor of a proportional counter can be computed, within the limits of the approximation that the Townsend coefficient is proportional to the average electron energy, expression (5.5) (Korff, 1955). Since $1/\alpha$ is the mean free path for ionization, the average energy acquired from the electric field E by an electron between collisions is E/α ; from (7.1):

$$\epsilon = \sqrt{\frac{CV_0}{2\pi \epsilon_0 kN} \frac{1}{r}},$$

therefore:

$$\alpha(r) = \sqrt{\frac{kNCV_0}{2\pi \epsilon_0} \frac{1}{r}}. \quad (7.3)$$

The gain of the counter can then be obtained by integrating over the useful field region. Assuming that the avalanche multiplication begins at a critical distance r_c from the wire centre at which the electric field exceeds a critical value E_c :

$$M = e \int_a^{r_c} \alpha(r) dr, \quad (7.4)$$

recalling the definition of threshold voltage V_T :

$$E_c = \frac{CV_T}{2\pi \epsilon_0 a} \quad \text{and} \quad \frac{r_c}{a} = \frac{V_0}{V_T}; \quad (7.5)$$

substituting (7.3) in (7.4), integrating and using (7.5):

$$M = e^{2\sqrt{\frac{kNCV_0 a}{2\pi \epsilon_0}} \left(\sqrt{\frac{V_0}{V_T} - 1} \right)}. \quad (7.6)$$

For $V_0 \gg V_T$, the multiplication factor is seen to depend exponentially on the charge per unit length $Q = CV_0$:

$$M = K e^{HC V_0}. \quad (7.7)$$

Once the threshold voltage has been determined, the multiplication factor can be computed using the values of k given in Table 5.2. Figure 7.6 (Staub, 1953), shows

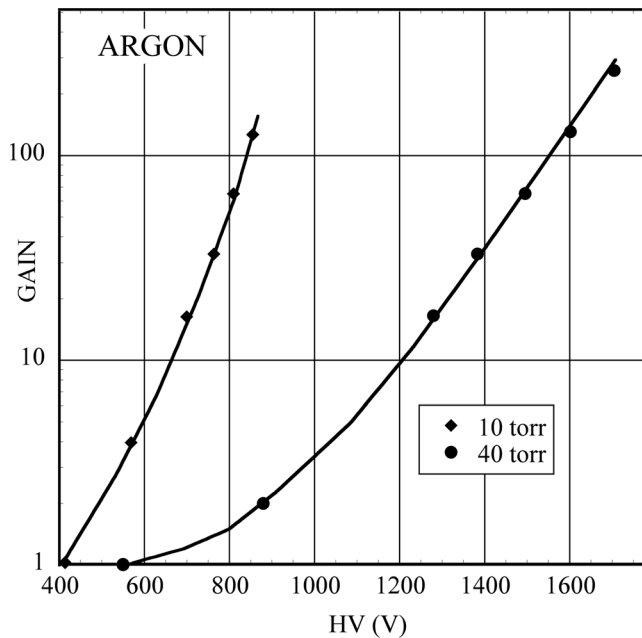


Figure 7.6 Comparison between the gain computed with Korff's approximation and measurements. Data from Staub (1953). By kind permission of J. Wiley & Son.

the computed and measured gains for argon at two values of pressure (in cm Hg): the agreement is excellent for moderate gains.

Many authors have developed alternative formulations to the original Rose and Korff expression, aiming at improving the agreement with experimental data; a summary and extended bibliography can be found in Bambynek (1973).

The expressions are adequate for a qualitative understanding of the proportional counters' operation. For gain values above 10^4 , however, the approximations used for α are not justified; a summary of more detailed calculations by different authors is given in Palladino and Sadoulet (1975).

Methods of calculation of the electric field and signal induction in cylindrical counters with wire cathodes are discussed in Szarka and Povinec (1979), and for counters having rectangular cross section in Tomitani (1972); the results can be used to optimize the design of the counters, and easily extended to multi-element detectors consisting of wire-delimited identical adjacent cells as implemented in volumetric multi-wire drift chamber arrays.

A concise parametric model of the avalanche processes in gas counters is given in Bateman (2003); the discussion covers a range of detectors of different geometry. Approximate expressions of gain for cylindrical wire counters, micro-strip chambers, point anode and parallel plate counters are provided,

and permit one to analyse experimental data obtained in a range of gas fillings and operating conditions.

7.2 Absolute gain measurement

The detector multiplication factor, or gain, is defined as the ratio between the collected charge on each electrode, positive on the cathode and negative on the anode, and the primary ionization charge. As discussed in the next section, due to the large difference in the mobility of electrons and ions, and to the characteristics of the amplifier, the fast component of the detected charge is only a fraction of the total. Although an electronics gain calibration can be done by injecting a known amount of charge into the amplifier-pulse height measurement chain, the result depends on the time constants of the circuits, it is affected by the generally unknown detector capacitance, and only provides relative values.

Alternative methods of absolute gain measurements are widely used. The first consists of a direct measurement of the detector current, under uniform irradiation, making a complete voltage–current characterization, as the one shown in Figure 7.5: the gain at a given voltage is then the ratio between the current recorded at that voltage and the one corresponding to the ionization chamber plateau. The method requires high source intensities and/or heavily ionizing particles in order to measure the ionization current accurately.

Alternatively, one can realize simultaneous or consecutive measurements of the current I and rate R under exposure to radiation with a known ionization yield, as for example a soft X-ray source. The absolute gain M at a given voltage is then:

$$M = \frac{I}{NeR},$$

where the average ionization yield for each event, N , can be estimated from expression (2.3). Requiring efficient detection of each ionizing event for the estimate of R , the method can only be used when sufficiently high gains can be attained.

7.3 Time development of the signal

As indicated, charge multiplication begins at a few wire radii, i.e. typically less than 50 μm from the anode surface. Assuming a value of 5 $\text{cm}/\mu\text{sec}$ for the drift velocity of electrons in this high field region, it appears that the whole process of multiplication takes place in less than 1 ns: after this time, all electrons in the avalanche have been collected on the anode, and the positive ion sheath drifts towards the cathode at decreasing velocity. The detected signal, negative on the

anode and positive on the cathode, is the consequence of the change in energy of the system due to the movement of charges. The simple electrostatic considerations discussed in Chapter 6 show that if a charge Q is moved by dr in a system of total capacitance LC (where L is the length of the counter), the induced signal is:

$$dv = \frac{Q}{LCV_0} \frac{dV}{dr} dr. \quad (7.8)$$

Electrons in the avalanche are produced very close to the anode (half of them in the last mean free path); therefore their contribution to the total signal is very small: positive ions, instead, drift across the counter and generate most of the signal. Assuming that all charges are produced at a distance λ from the wire, the electron and ion contributions to the signal on the anode are, respectively:

$$v^- = -\frac{Q}{LCV_0} \int_a^{a+\lambda} \frac{dV}{dr} dr = -\frac{Q}{2\pi\epsilon_0 L} \ln \frac{a+\lambda}{a},$$

$$v^+ = \frac{Q}{LCV_0} \int_{a+\lambda}^b \frac{dV}{dr} dr = -\frac{Q}{2\pi\epsilon_0 L} \ln \frac{b}{a+\lambda}.$$

The total maximum signal induced on the anode is then:

$$v = v^+ + v^- = -\frac{Q}{2\pi\epsilon_0 L} \ln \frac{b}{a} = -\frac{Q}{LC}$$

and the ratio of the two contributions:

$$\frac{v^+}{v^-} = \frac{\ln(a+\lambda) - \ln a}{\ln b - \ln(a+\lambda)}.$$

Substituting in the previous expression typical values for a counter, $a = 10 \mu\text{m}$, $\lambda = 1 \mu\text{m}$ and $b = 10 \text{mm}$, one finds that the electron contribution to the signal is about 1% of the total; it is therefore, in general, neglected for most practical purposes.

The time development of the signal can be deduced assuming then that ions leaving the surface of the wire with constant mobility are the only contribution. In this case, integration of (7.8) gives for the signal induced on the anode the expression:

$$v(t) = -\int_0^t dv = -\frac{Q}{2\pi\epsilon_0 L} \ln \frac{r(t)}{a}. \quad (7.9)$$

From the definition of mobility, it follows that

$$\frac{dr}{dt} = \mu^+ \frac{E}{P} = \frac{\mu^+ CV_0}{2\pi\epsilon_0} \frac{1}{r}$$

and therefore

$$\int_a^r r dr = \frac{\mu^+ CV_0}{2\pi\epsilon_0} \int_0^t dt,$$

$$r(t) = \sqrt{a^2 + \frac{\mu^+ CV_0}{\pi\epsilon_0} t}.$$

Substituting in (7.9):

$$v(t) = -\frac{Q}{4\pi\epsilon_0 L} \ln\left(1 + \frac{\mu^+ CV_0}{\pi\epsilon_0 a^2} t\right) = -\frac{Q}{4\pi\epsilon_0 L} \left(1 + \frac{t}{t_0}\right), \quad (7.10)$$

and the corresponding current:

$$i(t) = LC \frac{dv(t)}{dt} = -\frac{QC}{4\pi\epsilon_0} \frac{1}{t_0 + t},$$

$$t_0 = \frac{\pi\epsilon_0 a^2}{\mu^+ CV_0}.$$

The current is maximum for $t = 0$:

$$i_{\text{MAX}} = i(0) = -\frac{\mu^+ QC^2 V_0}{4\pi^2 \epsilon_0^2 a^2}. \quad (7.11)$$

The total drift time of the ions, T^+ , is obtained from the condition $r(T^+) = b$:

$$T^+ = \frac{\pi\epsilon_0(b^2 - a^2)}{\mu^+ CV_0},$$

$$v(T^+) = -\frac{Q}{LC}.$$

Due to the high initial velocity of the ions in the field around the anode, the signal growth is very fast at short times: about one half of the signal develops in a fraction of time corresponding to the ratio of the anode to cathode radius:

$$v\left(\frac{a}{b} T^+\right) \approx \frac{Q}{2LC}.$$

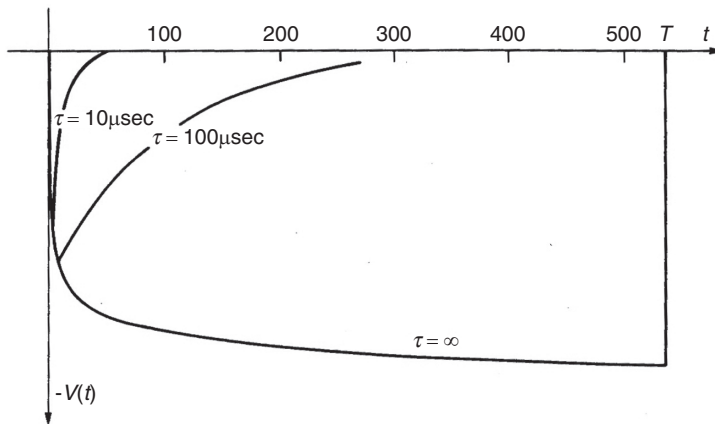


Figure 7.7 Time evolution of the voltage pulse on the anode, for several values of the time constant of the load.

With the aim of increasing the rate capability of the counter, it is normal practice to terminate the anode with a resistor R , such that the signal is shaped with a time constant $\tau = RC$; short pulses can be obtained using low impedance terminations, at the cost of a reduced amplitude.

Figure 7.7 is an example of time development of the signal computed for an argon-filled counter at STP, with $a = 10 \mu\text{m}$, $b = 8 \text{ mm}$, $C = 8 \text{ pF/m}$ (from (7.2)) and $\mu^+ = 1.7 \text{ cm}^2\text{s}^{-1}\text{V}^{-1}$ (from Table 4.2); for a typical operational voltage $V_0 = 3 \text{ kV}$, the total length of the pulse is $T = 550 \mu\text{s}$.

Substituting the numerical values of the previous example, and assuming $Q = 10^6 e$ (where e is the electron charge) one gets $I_{\text{MAX}} \sim 10 \text{ nA}$, a typical value for the operation of proportional counters.

7.4 Choice of the gas filling

Avalanche multiplication occurs in all gases; virtually any gas or gas mixture can be used in a proportional counter. In most cases, however, the specific experimental requirements restrict the choice to selected families of compounds; low working voltage, high gain operation, good proportionality, high rate capabilities, long lifetime and fast recovery are examples of sometimes conflicting requirements. In what follows, the main properties of different gases in the performance of proportional counters are briefly outlined; a more detailed discussion can be found in the literature (Curran and Craggs, 1949; Korff, 1955; Franzen and Cochran, 1956).

As discussed in Chapter 5, avalanche multiplication occurs in noble gases at much lower fields than in complex molecules: this is a consequence of the many

non-ionizing energy dissipation modes available in polyatomic molecules. Convenience of operation suggests then using a noble gas as the main filling; addition of other components, for the reasons to be discussed below, will of course increase the multiplication threshold voltage. The choice within the family of noble gases is then dictated, at least for the detection of minimum ionizing particles, by the requirement of a high specific ionization; with reference to Table 2.1, and disregarding xenon or krypton for economic reasons, the choice falls naturally on argon.

Excited and ionized atoms form in the avalanche process; the excited noble gases return to the ground state only through a radiative process, and the minimum energy of the emitted photon (11.6 eV for argon) is well above the ionization potential of any metal constituting the cathode (7.7 eV for copper). Photoelectrons can therefore be extracted from the cathode, and initiate a new avalanche very soon after the primary; an argon-operated counter generally does not allow gains in excess of a few hundred without entering into permanent discharge.

Positive ions produced in the avalanche migrate to the cathode and are there neutralized by extracting an electron; the balance of energy is either radiated as a photon, or by secondary emission of electrons from the metal surface. Both processes result in a delayed spurious avalanche: even for moderate gains, the probability of the processes discussed is high enough to induce a permanent regime of discharge. Polyatomic molecules have a different behaviour, especially when they contain more than four atoms; the presence of non-radiative excited states (rotational and vibrational) allows the absorption of photons in a wide energy range (see Chapter 3). For methane, for example, absorption is very efficient in the range 7.9 to 14.5 eV, which covers the range of energy of photons emitted by argon. This is a property of most organic compounds in the hydrocarbon and alcohol families, and of several inorganic compounds like freons, CO₂, CF₄ and others; these molecules dissipate the excess energy by elastic collisions or by dissociation into simpler radicals. The same behaviour is observed when a polyatomic ionized molecule neutralizes at the cathode: secondary emission is very unlikely. Even small amounts of a polyatomic quencher added to a noble gas change the operation of a counter, because of the lower ionization potential that results in a very efficient ion exchange process. Good photon absorption and suppression of the secondary emission allows gains of 10⁵–10⁶ to be reached before discharge.

Argon–methane in the volume percentages 90–10 (the so-called P10 mixture) is widely used in wire proportional counters. The quenching efficiency of a polyatomic gas increases with the number of atoms in the molecule; isobutane (i-C₄H₁₀) is often used for high-gain, stable operation. Secondary emission has been observed, although with low probability, when using as quenchers simpler molecules like carbon dioxide, which may occasionally result in discharges.

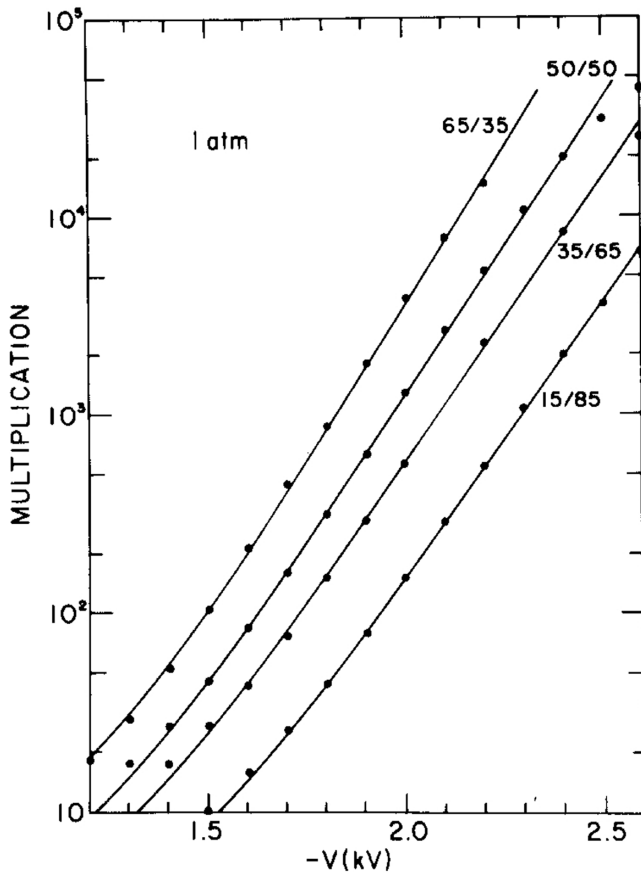


Figure 7.8 Proportional counter gain in argon–ethane mixtures (Behrends and Melissinos, 1981). By kind permission of Elsevier.

Comparative studies of gain and energy resolution of proportional counters with argon–methane and argon–ethane gas fillings in a range of conditions can be found, for example, in Behrends and Melissinos (1981). Figure 7.8 and Figure 7.9 are examples of measured gain in argon–ethane in a range of percentages and pressures; solid lines are fits using the Rose and Korff expression.

Addition of small quantities of electro-negative gases, like freons (CF_3Br in particular) or ethyl bromide ($\text{C}_2\text{H}_5\text{Br}$) allows one to reach a saturated mode of operation in the so-called ‘magic gas’, see Section 8.6 (Bouclier *et al.*, 1970). Aside from their photon-quenching capability, electro-negative gases capture free electrons, forming negative ions that cannot induce avalanches in the field values normally met in a proportional counter. If the mean free path for electron capture is shorter than the distance from anode to cathode, electrons liberated at the cathode by the described processes have very little probability of reaching the anode, and

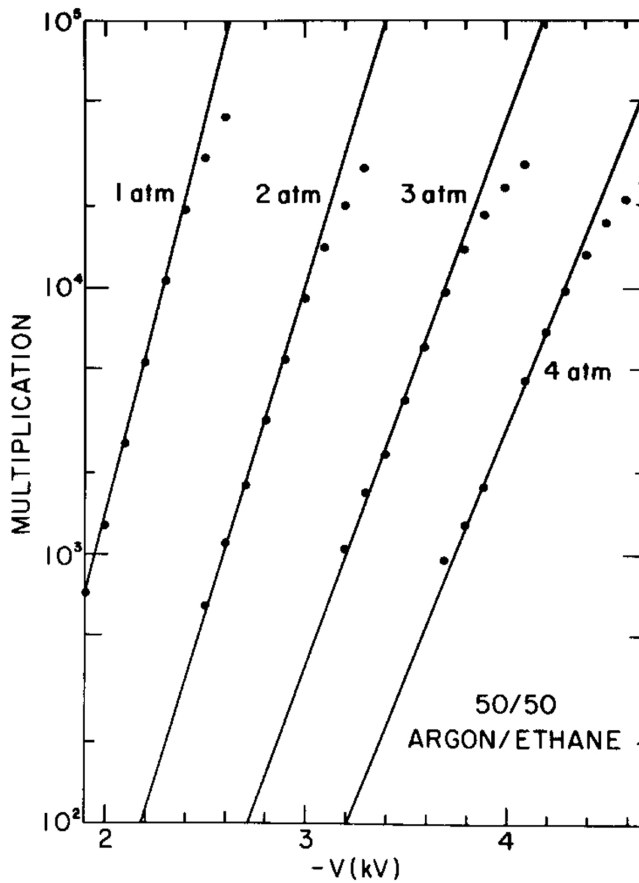


Figure 7.9 Proportional counter gain in a range of pressures in a 50–50 argon–ethane mixture (Behrends and Melissinos, 1981). By kind permission of Elsevier.

gains around 10^7 can be safely obtained before discharge or breakdown. To preserve detection efficiency, however, only limited amounts of electro-negative gases can be used (Breidenbach *et al.*, 1973).

Unfortunately, the use of polyatomic organic gases can have a dramatic consequence on the lifetime of counters, when high fluxes of radiation are detected, in a degenerative process appropriately named ageing. This subject will be covered in Chapter 16.

7.5 Energy resolution

The process of avalanche multiplication, statistical in nature, introduces fluctuations to the average charge gain of a counter. Usually of small relevance in the

detection of fast charged particles, due to the large spread in the primary ionization yield, avalanche fluctuations have a dominant effect in determining the energy resolution of proportional counters in the detection of soft X-rays.

If N is the average number of electron–ion pairs released in the gas and M the counter's gain, the relative pulse height resolution can be written as:

$$\left(\frac{\sigma_P}{P}\right)^2 = \left(\frac{\sigma_N}{N}\right)^2 + \left(\frac{\sigma_M}{M}\right)^2. \quad (7.12)$$

The terms in the expression correspond to the squared sum of the variance in the number of ionization electrons and of the multiplication factor, respectively. Averaged over the N single electron avalanches of size A_i , the gain M can be written as:

$$M = \frac{1}{N} \sum_{i=1}^N A_i = \bar{A}$$

and its variance

$$\sigma_M^2 = \left(\frac{1}{N}\right)^2 \sum_{i=1}^N \sigma_A^2 \text{ or } \left(\frac{\sigma_M}{M}\right)^2 = \frac{1}{N} \left(\frac{\sigma_A}{\bar{A}}\right)^2. \quad (7.13)$$

As shown in Section 5.4, for a Furry statistics the variance of the single electron avalanche fluctuation is equal to the average avalanche size, $\sigma_A = \bar{A}$, while for a Polya gain distribution it can be written as:

$$\left(\frac{\sigma_A}{\bar{A}}\right)^2 = \frac{1}{\bar{A}} + \frac{1}{1+\theta}, \quad (7.14)$$

which reduces to the previous for $\theta = 0$ and large values of \bar{A} . In both cases, the avalanche fluctuations increase with the avalanche size (the gain of the counter).

As discussed in Section 3.6, for totally absorbed X-rays, the variance in the number of electron–ion pairs can be written as: $\sigma_N^2 = F N$, an expression that takes into account the statistics of energy loss for soft X-rays; the Fano factor F (≤ 1) has a value that depends on the gas (Fano, 1963). Combining the two expressions, and adding a term describing the electronics noise:

$$\frac{\sigma_P}{P} = \sqrt{\frac{1}{N}(F + b)} + f(P). \quad (7.15)$$

Figure 7.10 shows qualitatively the dependence of the resolution on the gain of a counter, assuming an exponentially decreasing noise spectrum and $N = 100$; the best resolution is obtained at the lowest gains for which the noise contribution becomes unimportant. Figure 7.11 is an example of energy resolution for 5.9 keV

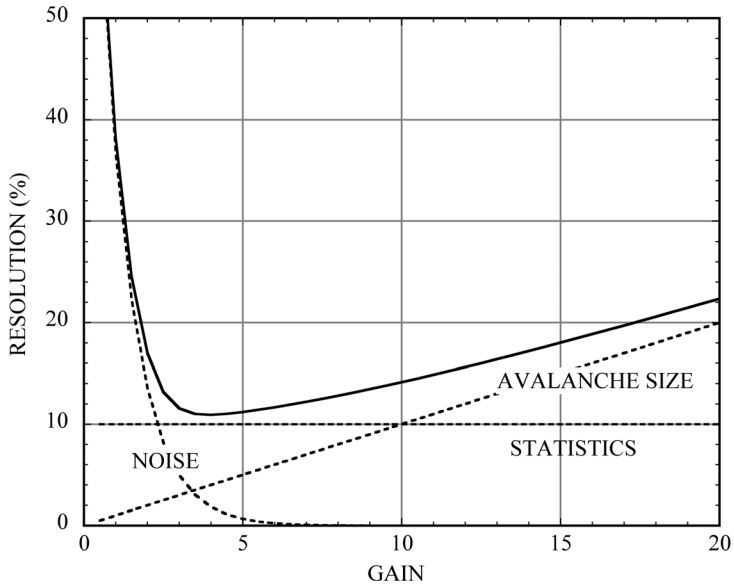


Figure 7.10 Qualitative dependence of a proportional counter resolution on gain due to various dispersive factors.

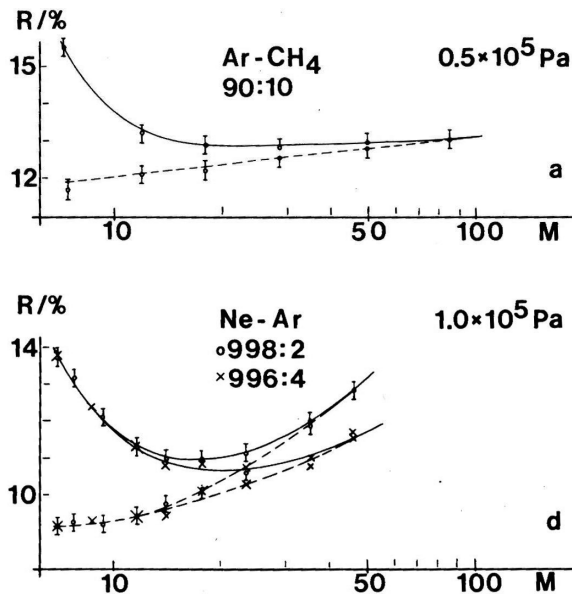


Figure 7.11 Measured energy resolutions FWHM at 5.9 keV as a function of gain for two gas mixtures (Järvinen and Sipilä 1982). By kind permission of Elsevier.

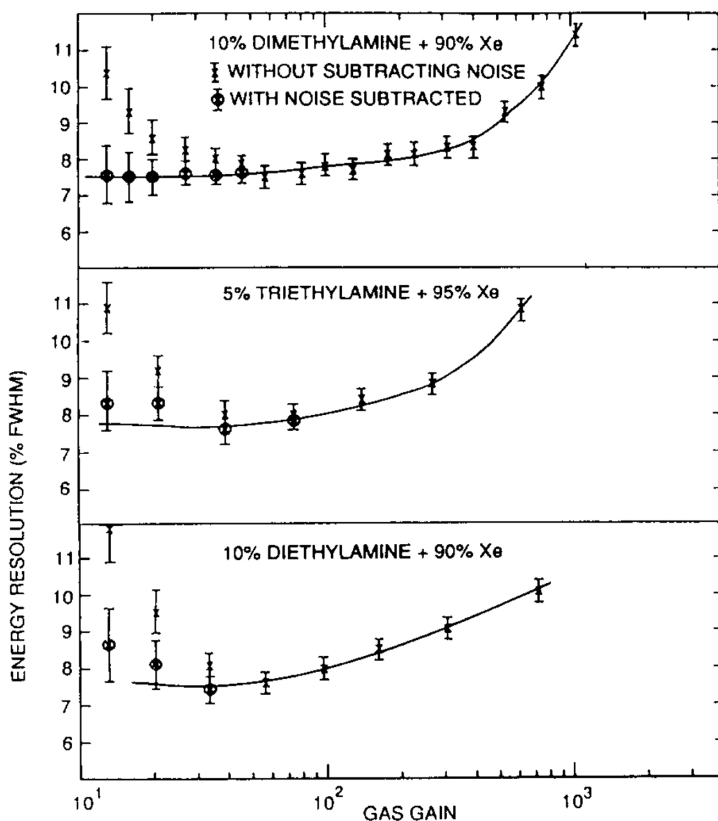


Figure 7.12 Energy resolution for 22 keV X-rays in several mixtures of xenon with low-ionization potential vapours (Ramsey and Agrawal, 1989). By kind permission of Elsevier.

X-rays, measured in the same counter with argon–methane or neon–argon fillings; the characteristic dependence of resolution on gain as well as the improvement with the second mixture, satisfying the Penning condition (see Section 5.3) are clearly seen (Järvinen and Sipilä, 1982). Detailed studies of resolution in Penning mixtures can be found in Sipilä and Kiuru (1978); Agrawal and Ramsey (1989); Agrawal *et al.* (1989); Ramsey and Agrawal (1989). Figure 7.12, from the last reference, is an example of gain dependence of energy resolution for mixtures of xenon and several photosensitive vapours, which satisfy the Penning condition thanks to their very low ionization potential. Using these quenchers has also the advantage of lowering the operating potential as compared to standard mixtures.

Many authors have studied the effect on resolution of geometrical factors in the counter construction and operation. Figure 7.13 is an example of computed dependence of resolution on the anode wire diameter and gas pressure for argon and methane, at a mean gain value of 100 (Alkhozov 1969). More detailed

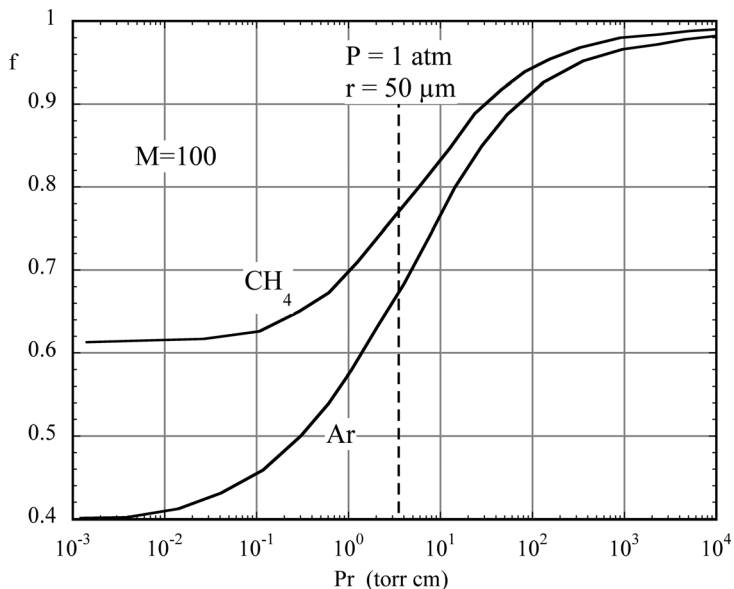


Figure 7.13 Relative variance of the gas amplification factor at an average gain of 100, computed as a function of the product between wire diameter r and gas pressure P . The dashed line corresponds to a typical choice of parameters in a counter (Alkhazov, 1969). By kind permission of Elsevier.

calculations are given in a later work by the same author (Alkhazov, 1970). It should be noted, however, that practical constraints limit the range of parameters that can be adopted for a proportional counter operation.

7.6 Scintillation proportional counters

As discussed above, the avalanche charge multiplication adds dispersions to the energy resolution, increasing with the charge gain. Detection of the charge before or very close to the onset of charge multiplication provides in principle the best resolution, close to the statistical limit; due to limitations imposed by electronics noise, this is hardly possible for small ionization yields such as those released by soft X-rays. A family of gaseous detectors, named gas scintillation proportional counters (GSPC), achieve the goal detecting, by optical means, the signals provided by secondary photon emission at fields below the onset of charge multiplication.

As discussed in Section 5.2, the inelastic collisions between electrons and molecules at moderate values of the electric field result in the creation of excited states, which return to the ground level with the emission of photons of wavelengths characteristic for each gas. The light yield increases exponentially with the

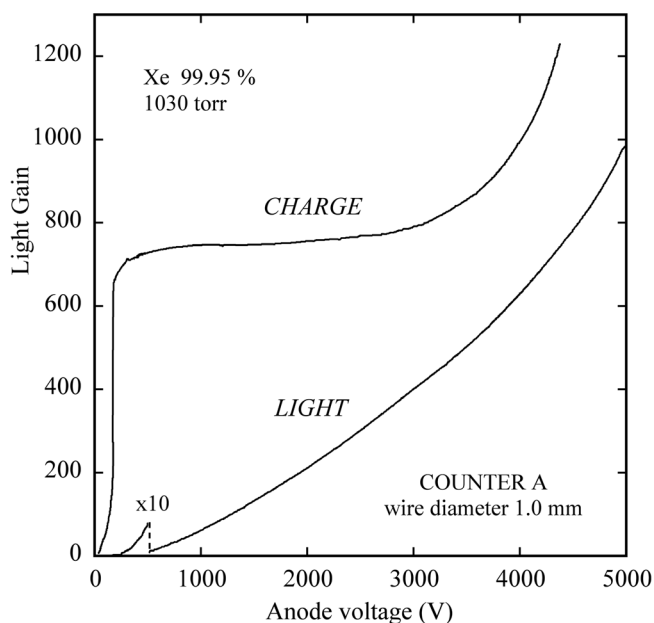


Figure 7.14 Charge and light gain measured with a scintillation proportional counter as a function of anode voltage (Policarpo *et al.*, 1972). By kind permission of Elsevier.

field, and is very copious approaching the charge multiplication threshold, as shown in Figure 7.14 (Policarpo *et al.*, 1972).

An example of a scintillation proportional counter, optimized for the detection of photons emitted by electrons approaching the anode, is shown in Figure 7.15 (Policarpo *et al.*, 1974). A spherical anode, mounted on a tip, is centred on a structure coupled to a photomultiplier through UV-grade windows on each side; the windows can be coated with a wavelength shifter to increase the quantum efficiency of the system. With a xenon filling at atmospheric pressure, the counter provides the pulse height spectra shown in Figure 7.16 for three soft X-ray lines: 227 eV, 1.49 keV and 5.9 keV, respectively (Policarpo *et al.*, 1974). The energy resolution for the 5.9 keV line is 8% FWHM, close to the statistical limit for xenon (6.5%, see Table 3.1), and can be compared with the best value of around 11% quoted in the previous section for a charge-multiplying counter using Penning mixtures.

Other scintillation counter designs have been developed, depending on experimental needs, using parallel plate or multi-wire chamber structures, operated below charge multiplication; for a review see Policarpo (1977). Recent developments include high pressure and large volume detectors; coupled to solid-state light sensors, they have the advantage of being very compact and insensitive to external

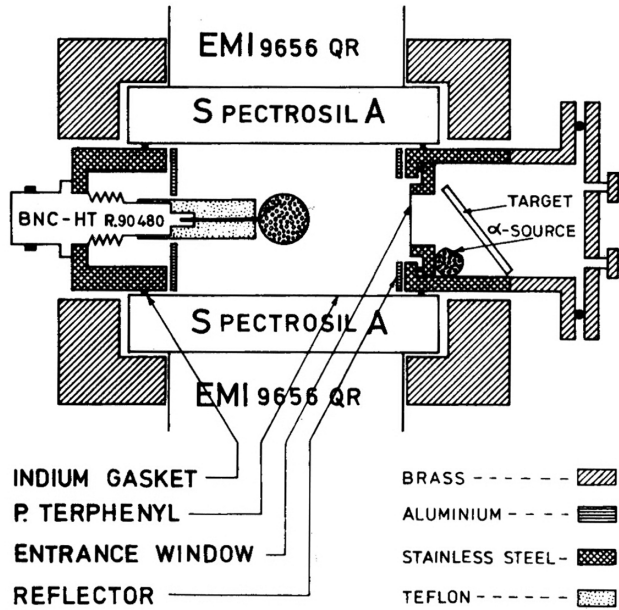


Figure 7.15 Schematics of a gas scintillation proportional counter with spherical anode and two photomultiplier light sensors (Policarpo *et al.*, 1974). By kind permission of Elsevier.

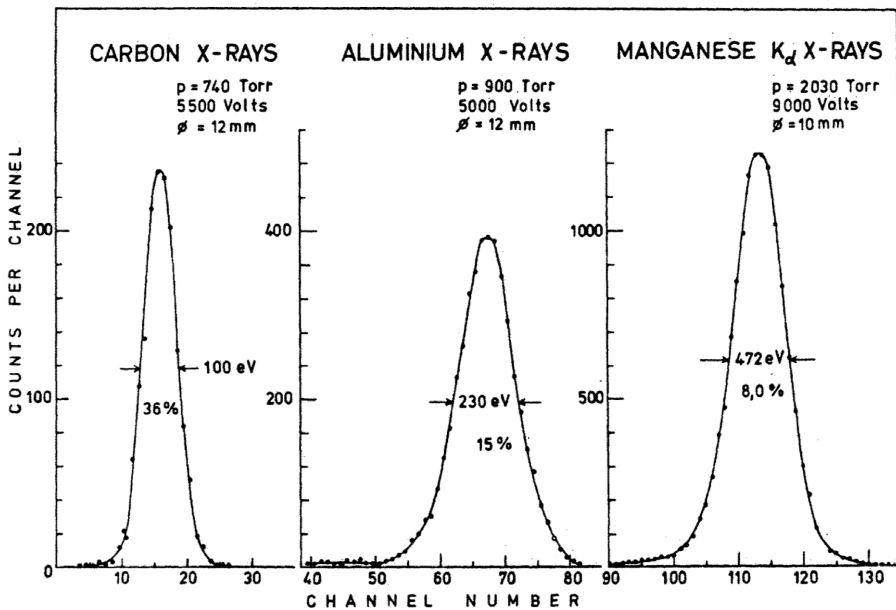


Figure 7.16 Energy resolution of a xenon-filled scintillation proportional counter for several X-ray energies (Policarpo *et al.*, 1974). By kind permission of Elsevier.

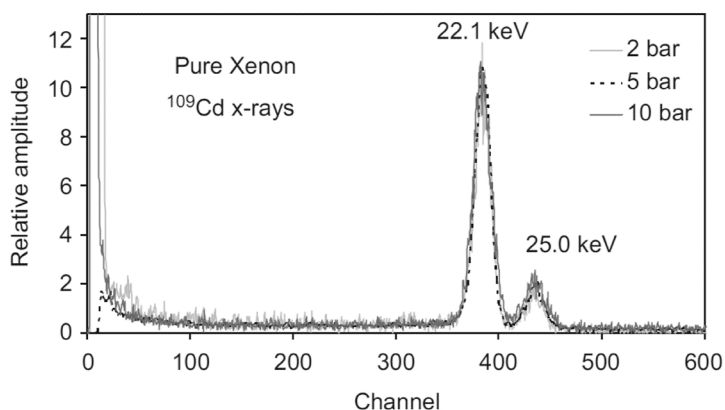


Figure 7.17 Energy resolution for ^{109}Cd X-rays of a Xe-filled GSPC at several pressures (Coelho *et al.*, 2007). By kind permission of Elsevier.

magnetic fields. Figure 7.17 is an example of energy resolution spectra measured in a xenon-filled GSPC with avalanche photodiode readout for ^{109}Cd X-rays at several pressures (Coelho *et al.*, 2007); the resolution for the 22.1 keV line is 4.5%, again close to the statistical limit (3.5%).

Methods for directly counting the number of primary ionization electrons have also been developed, making use of optical detection (Siegmond *et al.*, 1983) as well as charge detection with micro-pattern gaseous detectors, described in Chapter 13. Operation at low pressures allows spreading of the clusters by diffusion and detection of the arrival time of individual electrons; by using a dedicated algorithm to identify the peaks in the time-dispersed signal, single electron sensitivity could be reached (Pansky *et al.*, 1993); Figure 7.18 shows the energy spectra of sub-keV X-rays, measured by the electron counting method with optical detection. Results are similar for charge detection; the resolutions are close to the expected statistical values.

7.7 Space-charge gain shifts

During the avalanche development, the growth of a positive ion sheath around the wire results in a local drop of the electric field, with a consequent dynamic reduction of the amplification factor; the normal field is restored only when the ions leave the proximity of the wire and are neutralized at the cathode after several hundred microseconds. The gain is self-affected within each count, implying a loss of proportionality that reflects in a dependence of the gain-voltage characteristics from the initial ionization density, as clearly seen in the typical proportional counter response (Figure 7.5). When a counter is operated in the proportional or

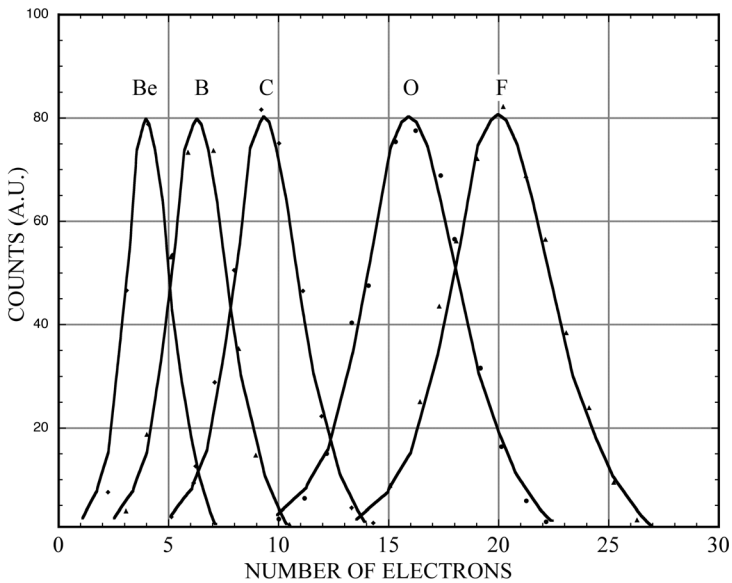


Figure 7.18 Energy resolution for ultra-soft X-rays measured with electron counting (Pansky *et al.*, 1993). By kind permission of Elsevier.

semi-proportional mode, the extension of the avalanche along the wire is rather small, between 0.1 and 0.5 mm, and therefore the field modification is confined to a small region of the counter. In Geiger–Müller operation, on the contrary, the avalanches spread all along the wire and the field in the whole counter is affected: for several hundred μsec no further detection is possible.

The proportional gain dependence on the detected charge density and production rate in wire counters has been studied theoretically and experimentally by many authors to explain observed gain non-uniformities and the appearance of distorted peaks in X-ray and α -particle spectrometry (Hendricks, 1969; Sipilä *et al.*, 1980; Mathieson 1986; Kageyama *et al.*, 1996). In the first reference, in particular, the gain shift dependence on the counter geometry (anode and cathode diameter) and operating pressure is discussed in detail; Figure 7.19 shows the computed relative gain variation as a function of anode wire radius for cylindrical counters with different cathode radii. As expected, the relative gain shift decreases with narrower tubes, due to faster ion collection; the reduction with the wire radius can be understood as due to a decrease of charge density because of the larger wire area. Practical considerations, as well as the possibility of reaching the gain required for detection, restrict the choice of geometry, however.

Following Hendrix, the approximate change of the anodic potential V_0 due to a flux R of ionizing radiation, each creating nMe charges in the avalanches is:

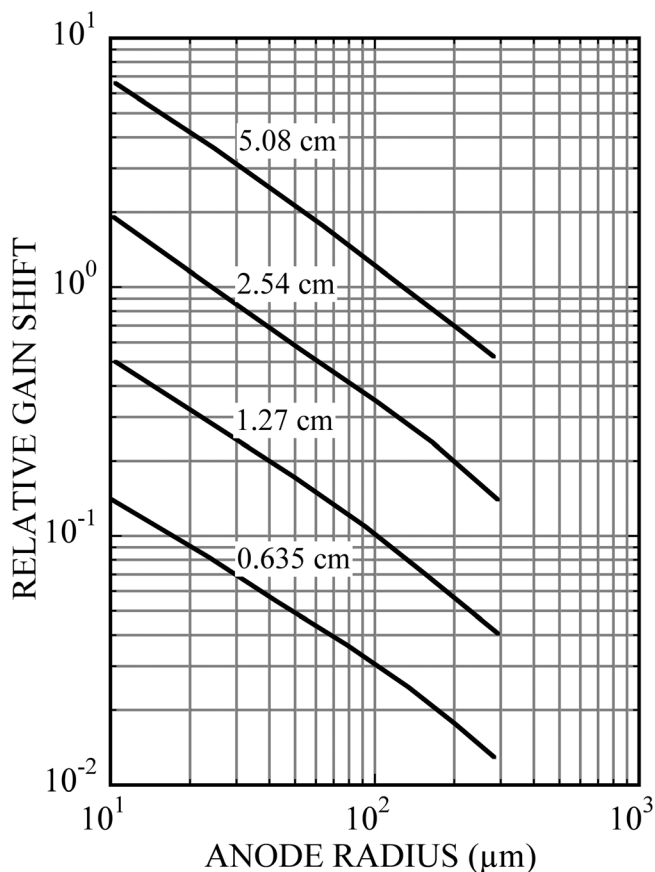


Figure 7.19 Computed relative gain shift in a cylindrical counter as a function of anode wire radius and several cathode radii (Hendricks, 1969). By kind permission of the American Institute of Physics.

$$\Delta V = V_0 - V = \frac{nMeRT^+}{4\pi^2\epsilon_0} = KMR,$$

$$K = \frac{neT^+}{4\pi^2\epsilon_0},$$

where T^+ is the total collection time of positive ions. Using the approximated expression (7.7) the gain at the rate R can then be written as:

$$M = M_0 e^{-\Delta V},$$

where M_0 is the gain at low rates; replacing in the previous expression:

$$\Delta V e^{\Delta V} = KM_0 R.$$

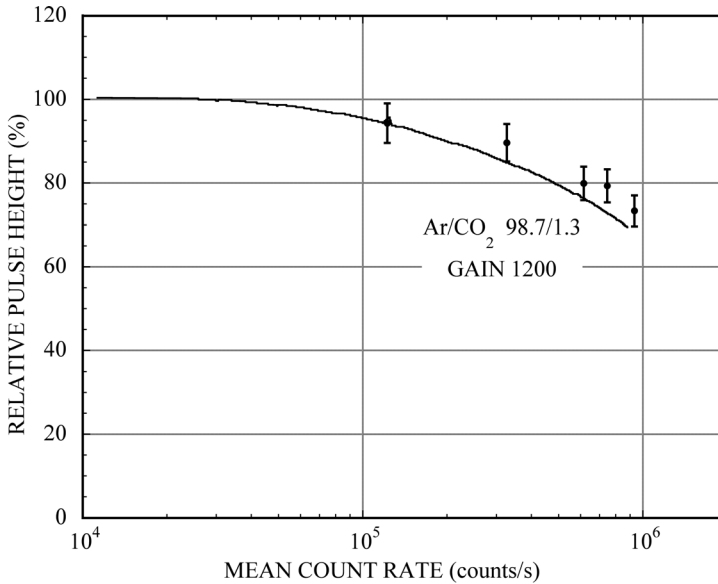


Figure 7.20 Computed (full curve) and measured relative gain as a function of counting rate (Sipilä *et al.*, 1980). By kind permission of Elsevier.

For small voltage variations, $e^{\Delta V} \approx 1$, $\Delta V \approx KM_0R$ and:

$$M = M_0 e^{-KM_0R}.$$

The good agreement between Hendricks' calculations and experiment is seen in Figure 7.20, showing the relative gain as a function of radiation measured with a single wire counter 2 cm in diameter and operated in Ar-CO₂ at a gain of 1200 (Sipilä *et al.*, 1980). In the experiment, the ⁵⁵Fe X-ray source used for the measurement was collimated on about 2 cm of wire; the gain is reduced to 70% of its low rate value at a flux of 5×10^4 counts/s per mm of wire.

For a given detector geometry, the relative gain reduction depends on the charge production rate, but is independent of the avalanche size, or initial gain, as seen in Figure 7.21 (Walenta, 1981); since the effect depends on the charge density, the rate is conventionally expressed per unit length of wire.

More exotic processes such as columnar recombination (Mahesh, 1976) and the formation of a sheet of polar molecules around the anode (Spielberg and Tsarnas, 1975) have been studied to explain some peculiarities of the observed gain reduction at low rates.

Despite decades of research, little progress has been done on rate capability with wire-based systems, confirming the fundamental nature of the space-charge limitation; Figure 7.22 (Aleksa *et al.*, 2000) is an example of the rate dependence of gain measured with the high-accuracy drift tubes of the ATLAS experiment at

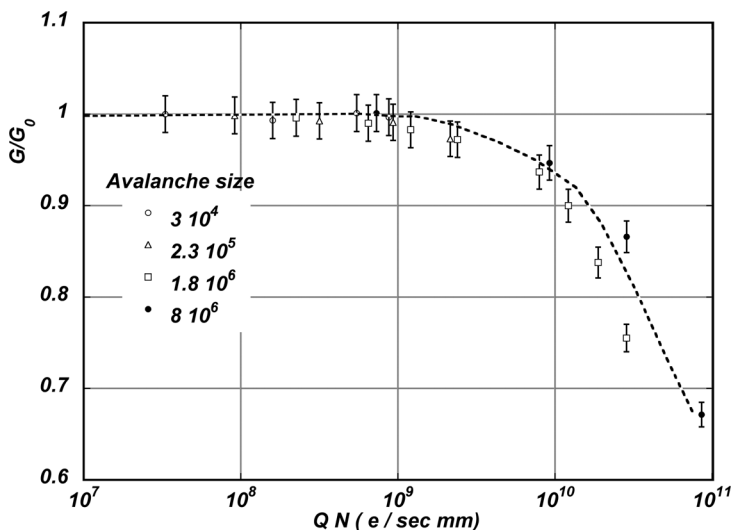


Figure 7.21 Normalized gain measured with a wire chamber as a function of particle flux, given in terms of charge production rate per mm of wire (Walenta, 1981). © The Royal Swedish Academy of Sciences. Reproduced by permission of IOP Publishing.

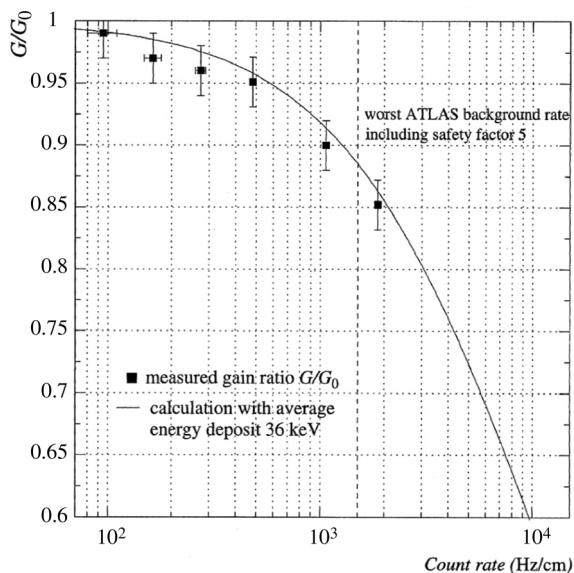


Figure 7.22 Relative gain dependence on particle flux in the high-accuracy drift tubes (Aleksa *et al.*, 2000). By kind permission of Elsevier.

CERN. In the conditions of the measurement, made with tubes 30 mm in diameter operated in Ar-CO₂ at 3 bars at a gas gain of 2×10^4 , the average avalanche size is around 3×10^7 ; a 10% gain reduction is observed at a charge density of around 3×10^9 electrons per second and mm of wire, close to the values indicated by the plot in Figure 7.21.

Apart from reducing the gain and therefore the detection efficiency, the accumulation of ions results in distortions of the drift field and consequent deterioration of localization accuracy, as discussed in the quoted reference.

As will be discussed in the next chapters, very similar gain reductions as a function of rate are observed in all wire-based gaseous detectors, multi-wire and drift chambers; the advent of a new generation of devices, the micro-pattern gas detectors, where the geometry and field configuration permit a faster collection and neutralization of positive ions, has substantially improved the rate capability of gaseous detectors (see Chapter 13).

7.8 Geiger and self-quenching streamer operation

The detected charge in a proportional counter has the characteristic dependence on applied voltage shown in Figure 7.5, going from charge collection, through proportional amplification and to a saturated gain, before reaching the breakdown limit. In special conditions, namely poorly quenched gases and/or low pressures, a different mechanism is observed (Geiger and Müller, 1928). Instead of a localized multiplication of the original ionization charge, a photon-mediated avalanche breeding sets in, propagating the charge multiplication in both directions along the wire, and eventually involving the whole counter. The discharge stops when the operating potential, usually applied to the tube through a high value resistor, drops below a critical value for maintaining the conditions of charge multiplication. This counting mode provides very large counting pulses, typically 10^9 to 10^{10} electrons even starting from small primary ionizations, down to a single electron, and is therefore widely in use for portable radiation monitors. Due to the long time needed to clear all ions and excited molecules produced in a discharge and restore the voltage, a millisecond or more, the rate capability of a Geiger counter is rather limited. Methods of extending the dynamic range of counters with corrections of dead-time losses are discussed in Jones and Holford (1981).

For a review on the Geiger–Müller process and operation of the counters see, for example, the reference book by Wilkinson (1950) and the more recent updates of the same author (Wilkinson, 1992; Wilkinson, 1996a; Wilkinson, 1996b; Wilkinson, 1999). The detection efficiency of counters with cathodes of different thickness is discussed in Watanabe (1999).

With the use of thick anode wires and operating in hydrocarbon-rich gas mixtures, a sudden appearance of very large signals was observed in multi-wire detectors, initially attributed to a transition to a Geiger discharge, limited in extension along the wire because of the quenching effect of the gas mixture used (Brehin *et al.*, 1975). However, further work led to the deduction that the large signals were rather due to a peculiar mode of discharge, propagating perpendicular to the wires and damped before reaching the cathodes; the process was appropriately named self-quenching streamers (SQS) (Alexeev *et al.*, 1980). The mechanism of streamer propagation was described in Section 5.5; in uniform fields, it leads to a discharge between electrodes. With wire counters, the backwards propagation of the streamer towards the cathode can stop in the decreasing electric field, providing large and saturated signals; this mode of operation is exploited in the family of devices named limited streamer tubes, discussed in detail in Chapter 11.

The transition from semi-proportional to SQS occurs when the avalanches exceed a certain size, and therefore takes place at different voltages depending on the initial ionization charge; the semi-proportional and SQS modes coexist over a short range of voltages, as seen in Figure 7.23 (Koori *et al.*, 1986b).

The mechanism of propagation of SQS requires the emission in the avalanches of photons capable of photo-ionizing one of the components of the gas mixture, and has been studied by many authors in a variety of conditions and gases (Koori *et al.*, 1986b; Kamyshov *et al.*, 1987; Koori *et al.*, 1989; Ohgaki *et al.*, 1990; Koori *et al.*, 1990). A quantitative theory of the photon-mediated transition and expressions for the gain in the SQS mode are given in De Lima *et al.* (1985) and compared with experimental measurements in Ohgaki *et al.* (1990).

Due to the limited extension of the avalanche charge in the SQS mode, as compared to a full Geiger, the rate capability is increased, as shown in Figure 7.24 (Nohtomi *et al.*, 1994). Given in γ -ray radiation exposure units (mR/h), the horizontal scale is not easily converted to the counting rate, but serves as relative comparison.

It should be noted that the SQS transition was controversially observed also in mixtures where the photon feeding mechanism is energetically not allowed (Koori *et al.*, 1991).

7.9 Radiation damage and detector ageing

Permanent deterioration of performances under long-term irradiation has been observed since the early development of proportional counters. In Geiger counters, due to the extreme charge densities, this was attributed to a change in the gas composition due to the breakdown of the organic quenchers used; further studies, however, demonstrated that the culprit was a deposition of hydrocarbon polymers

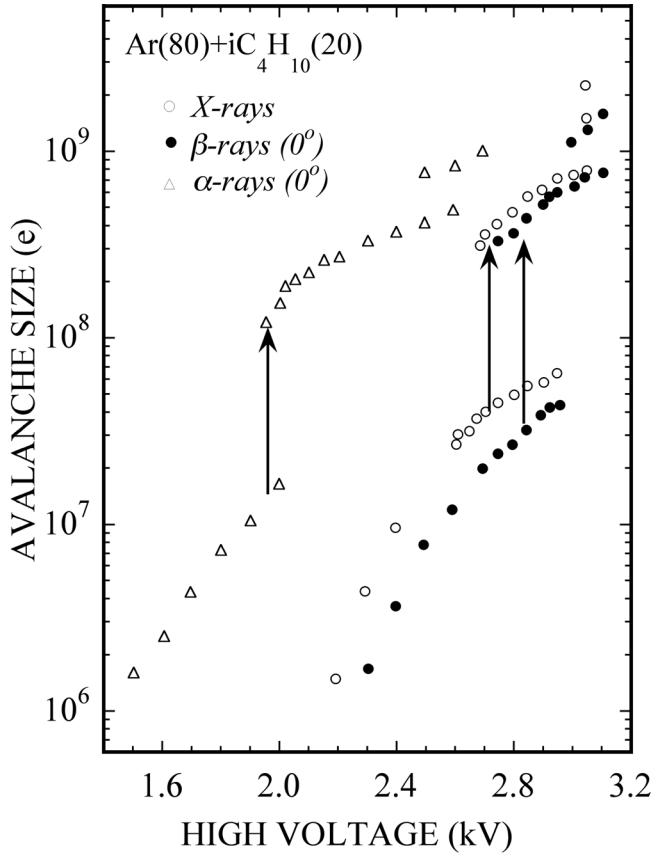


Figure 7.23 Transition from proportional to streamer regime with several ionizing sources (Koori *et al.*, 1986b). © The Japan Society of Applied Physics.

on electrodes. An example of deterioration is given in Figure 7.25, showing the singles counting rates as a function of voltage before and after several levels of irradiation (Farmer and Brown, 1948). Figure 7.26 is one of the first reported observations of ageing in a proportional counter with argon–methane filling, irradiated with a 5.9 keV X-ray source; the successive pulse height spectra, (a) to (e), show a progressive degradation of the resolution and the appearance of a second, lower amplitude peak (den Boggende *et al.*, 1969). By comparing the results obtained with different counters and gases, the authors inferred a gradual build-up of a thin, permanent and conductive deposit on the anode, which increases its diameter. The double peak can be explained by the higher rates on the wire side facing the source, resulting in faster ageing. A fluorescence surface analysis, and the recovery of the counter by thermal annealing, confirmed the presence of volatile carbon-rich deposits.

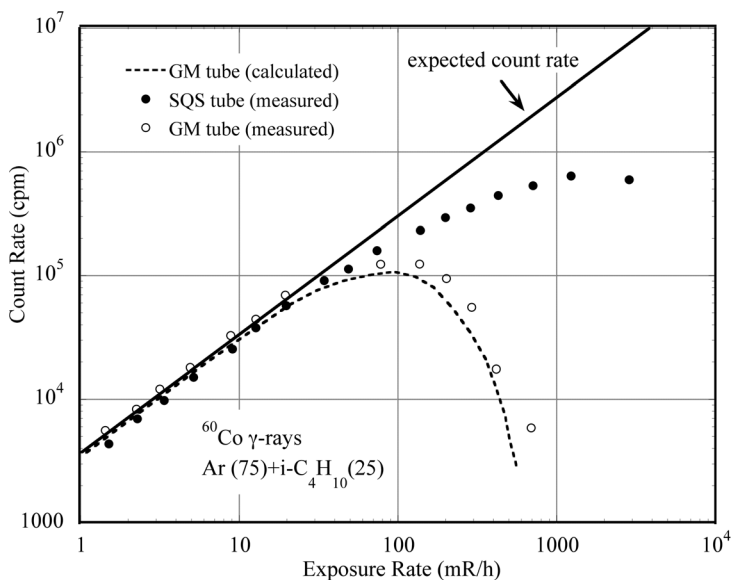


Figure 7.24 Comparison of rate capability of a counter operated in the full Geiger or the self-quenched streamer mode (Nohtomi *et al.*, 1994). By kind permission of Elsevier.

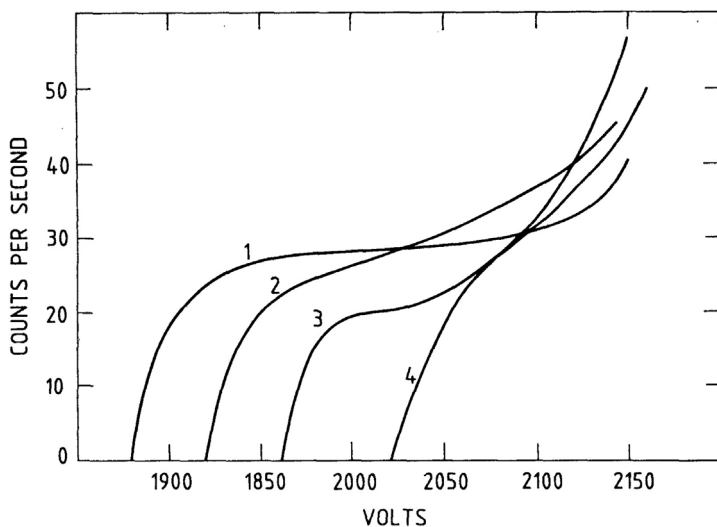


Figure 7.25 Progressive degradation of a Geiger counter with exposure to radiation. Curve 4 is the singles counting rate vs voltage measured after 10^8 counts (Farmer and Brown, 1948). By kind permission of the American Physical Society.

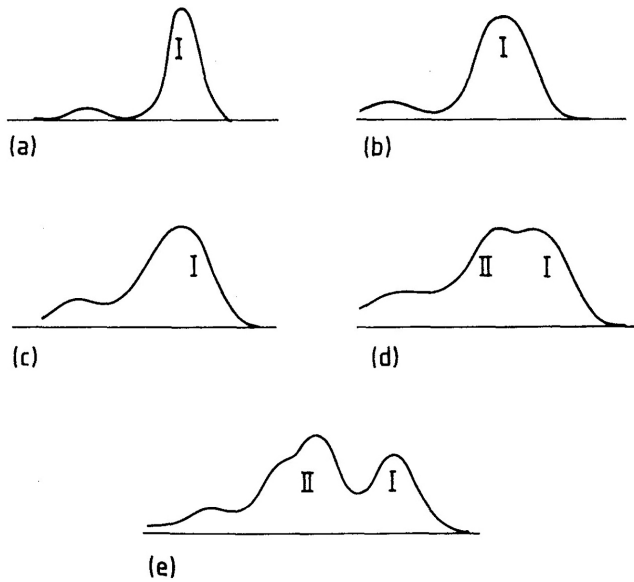


Figure 7.26 Time evolution of pulse height spectra for a counter irradiated with 5.9 keV X-rays (den Boggende *et al.*, 1969). © The Royal Swedish Academy of Sciences. Reproduced by permission of IOP Publishing.

As will be discussed extensively in Chapter 16, ageing effects have been encountered in the majority of gaseous detectors exposed to high radiation levels; in the presence of some pollutants, as for example residual oily vapours, the degradation can be disappointingly fast.